High Resolution Mapping of Compositional Differences at Electrode Interfaces by Electric Force Microscopy

G. A. Edwards, J. D. Driskell, A. J. Bergren, R. J. Lipert, and M. D. Porter*

Ames Laboratory-U.S.D.O.E. and the Institute for Combinatorial Chemistry
Iowa State University, Ames, Iowa 50011, mporter@porter1.ameslab.gov

ABSTRACT

This presentation examines the mechanistic basis for the ability of electric force microscopy (EFM) to map terminal group differences of spatially patterned organic monolayers. It compares the experimentally observed response to that from modeling calculations of the dipole moments of gold-bound adlayers prepared from a series of benzyl mercaptans, and serves as a starting point for gaining insight into the contrast mechanism. While preliminary, the results show that the dipole moment of the adlayer plays an important role in the contrast mechanism.

Keywords: electric force microscopy, monolayer, monomolecular film, dipole, modeling

1 INTRODUCTION

Scanning probe microscopic characterizations of organic thin films are widely utilized to investigate a range of interfacial processes (e.g., electrocatalysis, corrosion inhibition, conductivity of organic electronic devices, and biocompatibility).[1] Recent reports have described the ability of electric force microscopy (EFM) [2], an offshoot of atomic force microscopy, to map the terminal group differences of patterned organic monolayers that are buried under a thick (~500 nm) film of an organic polymer.[3] This presentation describes preliminary findings from experiments that seek to unravel the mechanistic basis of the contrast mechanism.

There are two steps in an EFM experiment. The first is a line-scan characterization of sample topography, which is usually collected by tapping mode. The electronic properties of the sample are interrogated on a second path across the sample in lift-mode (i.e., the tip is rastered across the same line at a constant tip-sample separation as determined by the previous topographic line-scan). In the second scan, a dc bias voltage is applied across a gold-coated tip and a grounded conductive substrate. The electrical forces (F_{elec}) interacting with the oscillating tip can be qualitatively represented in Eqn. 1 [4], where C is the capacitance of the media between the tip and sample, V_{sample} and V_{tip} are the voltages of the sample and tip, respectively, and z is the tip-sample separation. This formulation neglects contributions from the pyramidal-shape of the tip as well as the extended structure of the cantilever by treating the system as a parallel plate capacitor.

$$F_{elec} = \frac{\partial C}{\partial z}\frac{(V_{tip} - V_{sample})^2}{2} \quad (1)$$

Force measurements can be accomplished by monitoring the amplitude or phase shift of the tip oscillation, with phase shift being the more sensitive of the two approaches. The phase shift ($\Delta\Phi$) is proportional to the force gradient between the tip and sample, as shown in Eqn. 2. This equation indicates that a plot of $\Delta\Phi$ with respect to V_{tip} will have: 1) a parabolic shape with respect to a change in the tip-sample voltage; 2) a parabolic shape (e.g., the length of the *latus rectum*, *LR*) dependant on the capacitance of the media between the tip and sample; and 3) a minimum (i.e., the parabolic vertex) when V_{tip} and V_{sample} are identical. The adlayer results in a variation of the capacitance and voltage gradient between the tip and substrate, which gives rise to the image contrast mechanism.

$$\Delta\Phi \propto \frac{\partial F_{elec}}{\partial z} \propto \frac{\partial^2 C}{\partial z^2}\frac{(V_{tip} - V_{sample})^2}{2} \quad (2)$$

This paper utilizes a set of gold substrates, which are modified with five different *para*-substituted benzyl thiolates as a test system to begin to elucidate the interfacial properties that contribute to image contrast. Molecular modeling is utilized to predict how these monomolecular films will modify the electronic properties of the gold-air interface, such that the expected surface potential (ΔU_{model}) can be calculated. Electrochemical measurements are presented to confirm adlayer deposition, determine an experimental double layer capacitance (C_{dl}), and estimate adlayer surface coverage (Γ). This system of films is experimentally interrogated utilizing EFM to measure interfacial electronic properties. The model developed to predict EFM contrast is then compared to the experimentally observed values.

2 EXPERIMENTAL

2.1 Chemicals

Absolute ethanol was purchased from Aaper Alcohol. The *para-s*ubstituted benzyl mercaptans (H, *t*-butyl, Cl, F, and Br) and NaOH (semiconductor grade) were obtained from Aldrich. All chemicals were used as received.

2.2 Substrate and Monolayer Preparation

Template-stripped gold (TSG) was prepared as previously reported.[5,6] In brief, 300 nm of gold was resistively evaporated at a pressure of 7.5×10^{-7} Torr onto silicon(111) wafers (University Wafer) at 0.2 nm s^{-1}. Microscope slides (Fisher, 1 × 1 cm) were epoxied to the gold surface using Epo-Tek 377 (Epoxy Technology), and cured at 150 °C for 105 min. Samples were removed from the silicon wafer, and immediately immersed for 18 h in 1.0 mM ethanolic thiol solutions, removed from solution, rinsed copiously with ethanol, and dried. The resulting gold surface has an electrochemical roughness factor of 1.3.[6]

2.3 Molecular Modeling

Molecular models of the aromatic thiols were created by energy minimization using Chem3D Ultra 8.0.[7] The dipole moments were calculated utilizing the CS MOPAC Pro package. The MOPAC software employs the Parameterized Model (revision 3, PM3) to generate the potential energy function with a closed shell wave function. Dipole moments were calculated using the Milliken charge approximation. The three-dimensional molecular coordinates, in conjunction with the dipole vectors, were then utilized to determine the thickness and magnitude of the dipole moment (parallel to the alignment of the S-H bond) of the adlayers.

2.4 Electrochemistry

Electrochemical measurements were carried out using a CH Instruments model 600A potentiostat and a three-electrode cell with a platinum wire auxiliary electrode and a silver/silver chloride (saturated sodium chloride) reference electrode. All potentials are reported with respect to this reference. A solution of 0.5 M NaOH in high purity water was utilized for all experiments. Solutions were purged with nitrogen for 10 min prior to electrochemical measurements, and a blanket of nitrogen was held over the solution throughout each experiment.

The interfacial capacitance (C_{dl}) of the samples were determined utilizing cyclic voltammetry (CV).[8] CVs were collected at three sweep rates (50, 75, and 100 mV s^{-1}) by scanning between -0.3 V and +0.1 V. The double layer charging current at 0.0 V was used to calculate C_{dl}, which was independent of scan rate. Electrochemical measurements were also utilized to determine the surface concentration (Γ) of each adlayer by integrating the charge under the one-electrode desorption wave for the thiolate-based coating and accounting for the roughness factor of TSG.[8] Desorption voltammograms were collected by scanning cathodically from 0.0 V at 100 mV s^{-1}.

2.5 Electric Force Microscopy (EFM)

Data were collected with a Nanoscope 3A Multimode AFM, equipped with a signal access module for external control of V_{tip}. ΔΦ was measured while changing V_{tip} at a tip-sample separation of 100 nm, and an amplitude for the tip oscillation of ~15 nm. Cantilevers were purchased from MikroMasch (resonance frequency 265-400 kHz, force constant 20-75 N/m). These tips are coated with a 20-nm Cr film and then a 20-nm Au film, which resulted in a tip radius of ~50 nm. The sample compartment was purged with argon for 40 min prior to imaging, which was maintained for the duration of the experiments.

3 RESULTS

3.1 Molecular Modeling

Fig. 1 depicts the molecular model of benzyl mercaptan. In this visualization, the gold surface would be positioned on the right side of the image, aligned normal to the H-S bond. This architecture results in the aromatic ring aligned close to the surface normal, with the H-S bond then utilized as an internal marker for adlayer orientation.

Fig. 1: Molecular model of the energy-minimized benzyl mercaptan molecule. The orientation and confirmation of all the *p*-substituted benzyl mercaptans were consistent with this depiction.

The molecular coordinates of these molecules, after minimization, were employed to calculate the thickness of the adlayer. The thickness is given as the distance from the sulfur to the substituent (X) in the direction parallel to the H-S bond; it neglects the length of the gold-sulfur bond. These results are presented in Fig. 2A, and are consistent with expectations. That is, the monolayer with H in the *para* position has the lowest thickness, whereas the *t*-butyl containing adlayer has the largest thickness. In all cases, the results yield an adlayer in which the plane of the aromatic ring is tilted 11.6° ± 0.5° from the surface normal. These data are in general agreement with thicknesses determined by optical ellipsometry [9] and with the ring orientations found by molecular dynamics calculations [10] in similar systems. The molecular coordinates were also utilized to calculate both the closest packed area per molecule (A) and Γ for each of these adlayers, and are listed in Table 1. This analysis utilized the van der Waals radius of each atom, coupled with the projected ring orientation. The trend in molecular area follows intuition, such that the larger substituents (e.g., *t*-butyl) exhibit a larger surface area.

The most important results from these analyses are the dipole moments. Although the MOPAC software modeled the thiol precursors, the calculated dipole moment should be directly proportional to that of the corresponding adlayer because of the strong similarity in the thiolate linkages to the gold substrate. Data from X-ray photoelectron spectroscopy support this argument in that the positions of the S(2p) couplet are virtually identical for similar

systems.[11] This claim also applies to contributions from image dipoles created in the substrate by the adlayers. The results of the dipole moment calculations are shown in Fig. 2B and tabulated in Table 1. As evident, the fluorinated adlayer has the largest dipole moment, followed by the brominated, chlorinated, and hydrogenated adlayers; the *t*-butyl derivative has the lowest value. This trend follows insights based on electronegativity and charge separation considerations. It suggests that the fluorinated monolayer should induce the largest modulation of the voltage gradient between the tip and substrate.

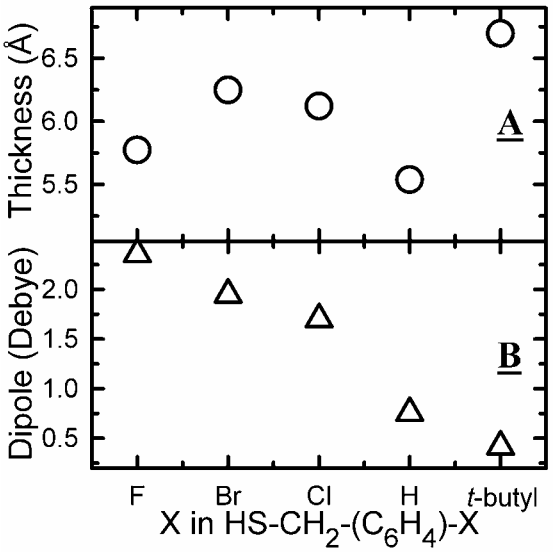

Fig. 2: (A) Calculated adlayer thickness (○) and (B) dipole moment (Δ) with respect to the surface normal.

The modeled data are utilized to calculate the theoretically predicted surface potential (ΔU_{model}) using Eqn. 3 [12], where A is in units of m^2, ε is the estimated relative permittivity of the monolayer (4.705) [13], ε_0 is the permittivity of free space (8.854×10^{-12} C m), $\mu_\perp$ is the dipole moment perpendicular to the surface (Debye), and ΔU is the expected change in surface potential with respect to the unmodified surface (V). The results of these calculations are presented in Table 1, and follow the trend based on the values of $\mu_\perp$.

$$\Delta U_{model} = 3.34 \times 10^{-30} \frac{\mu_\perp}{\varepsilon \varepsilon_0 A} \quad (3)$$

3.2 Electrochemistry

The C_{dl} and Γ of the adlayers were determined by electrochemistry. These results are presented in Table 1. As is evident, the values of C_{dl} are much lower than that of an uncoated gold electrode (~20 μF cm^{-2}).[8] Although nearly masked by the uncertainty of these measurements, the correlation of the capacitance values and substituent identity is close to that observed for the calculated dipole moments and surface potentials. That is, the C_{dl} for the adlayer with the *t*-butyl and hydrogen substituents are lower than those with the halogens in the *para* position. There is, however, one notable difference: the C_{dl}-value for the brominated adlayer is marginally less than that for the two remaining halogenated systems as well as that for the hydrogenated adlayer.

The values of Γ follow the same general trend as the theoretical values from the modeling calculations, with one exception: the brominated adlayer resulted in a higher coverage than the other adlayers. This discrepancy potentially stems from two factors: 1) the presence of faradic process upon adlayer desorption, and/or 2) incomplete electrochemical background subtraction. Experiments are being designed to examine the possibilities for the discrepancies in the C_{dl} and Γ findings.

3.3 EFM

Values of ΔΦ were measured as a function of V_{tip} at a constant lift height (100 nm). These results are plotted in Fig. 3, and summarized in Table 1 in terms of the experimentally determined surface potential (ΔU_{exp}) and the shape of the resulting profile (i.e., the length of the *LR*). In each case, the dependence of ΔΦ on V_{tip} exhibits a parabolic shape as predicted by Eqn. 2. The plots also show that the *t*-butyl monolayer has the most negative value of ΔU_{exp}, whereas the Cl-terminated monolayer has the most positive value.

Table 1: Summary of theoretical and experimental values related to EFM contrast mechanism for a series of *para*-substituted benzyl thiolate monolayers on gold.

	Modeling Results					Experimental Results			
Substituent	Thickness[a]	A[b]	Γ[c]	$\mu_\perp$[d]	ΔU_{model}[e,f]	C_{dl}[g]	Γ[c]	ΔU_{exp}[e]	*Latus Rectum*[e]
F	5.77	27.0	6.15	2.357	0.699	4.4 (0.6)	10.4 (0.5)	1.94	12.17
Br	6.25	30.2	5.49	1.947	0.516	3.8 (1.1)	13.9 (8.4)	1.23	11.35
Cl	6.12	28.8	5.76	1.700	0.472	4.1 (0.8)	10.2 (0.7)	2.18	11.08
H	5.54	24.8	6.69	0.755	0.243	4.0 (0.8)	11.5 (1.1)	-0.08	11.27
t-butyl	6.70	40.0	4.16	0.416	0.084	3.2 (0.7)	9.1 (1.4)	-0.21	12.24

[a] Å; [b] $Å^2$ $molecule^{-1}$; [c] mole cm^{-2}; [d] Debye; [e] V; [f] calculated using ε for all adlayers equal to 4.705 [13]; [g] μF cm^{-2}; error presented as one standard deviation for at least 8 samples.

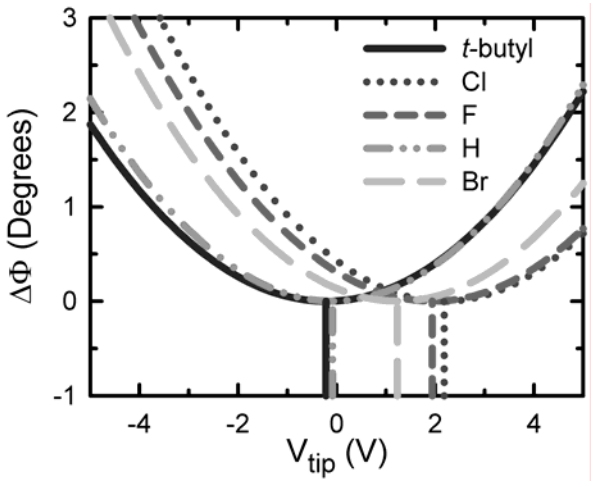

Fig. 3: Experimental $\Delta\Phi$ *vs*. V_{tip} with substrates of five different *para*-substituted benzyl mercaptan monolayers.

4 DISCUSSION

The curves in Fig. 3 yield several important observations. First, the V_{tip} at the parabolic vertex (ΔU_{exp}) of the plot for each adlayer is clearly different. Moreover, the trend in ΔU_{exp} (*t*-butyl < H < Br < F < Cl) closely, but not fully, matches with that for ΔU_{model} (*t*-butyl < H < Cl < Br < F). This agreement supports the possibility that the dipole moment is the major contributor to image contrast in EFM.

However, the lack of complete agreement points to several issues that require further investigation. From the prospective of modeling, the key limitation in the calculation of ΔU_{model} rests with the values for ε. Our analysis is presently limited by the lack of literature data for all the test systems. While ε for benzyl mercaptan has been reported [13], we have not been able to locate values for the remaining precursors. The literature for structurally similar compounds (e.g., benzenes and *para*-substituted toluenes) indicate that the value of ε may differ by up to 60%, indicating that only a qualitative comparison between ΔU_{model} and ΔU_{exp} can be reliably made at this time.

There are also several important refinements to address in the experimental area. First, the $\Delta\Phi$ curves of Fig. 3 have a parabolic shape that is dependant upon the capacitance of the media between the tip and substrate. However, the shapes, as judged from the *LR* values, do not track with the values of C_{dl}. We suspect that this situation reflects the presence of adventitious impurities adsorbed on the tip and sample. To address this issue, we are examining issues related to possible surface contaminates on the adlayer and tip as well as approaches to improve determination of C_{dl} and Γ, part of which will address methods to more reproducibly prepare the adlayers.

5 CONCLUSION

This paper has presented preliminary results that tested the effect of electronegative substituents on benzyl mercaptan-based monolayers assembled on gold surfaces. Electric force microscopy was utilized to interrogate the surface potential and capacitance of these adlayers. A theoretical model was developed to predict the expected trends in the EFM response. While preliminary, the results show that the dipole moment of the adlayer plays an important role in the contrast mechanism. Experiments to extend these first findings are planned.

ACKNOWLEDGEMENTS

This work was supported by the Basic Energy Sciences program of the U.S. Department of Energy. G.A.E. gratefully acknowledges a Conoco-Phillips graduate research fellowship. Valuable discussions with M. Gordon, I. Adamovic, and D. Zorn are also acknowledged. The Ames Laboratory is operated by Iowa State University for the U.S. Department of Energy under Contract W-7405-ENG-82.

REFERENCES

[1] Takano, H.; Kenseth, J. R.; Wong, S.-S.; O'Brien, J. C.; Porter, M. D. *Chem. Rev.* **1999**, 99, 2845-90.
[2] Fujihira, M. Annu. *Rev. Mater. Sci.* **1999**, 29, 353-80.
[3] a) Takano, H.; Porter, M. D. *J. Am. Chem. Soc.* **2001**, 123, 8412-3; b) Takano, H.; Wong, S.-S.; Harnisch, J. A.; Porter, M. D. *Langmuir* **2000**, 16, 5231-3.
[4] Sarid, D. *Scanning force microscopy: with applications to electric, magnetic, and atomic forces*; Oxford University Press: New York, 1994.
[5] Stamou, D.; Gourdon, D.; Liley, M.; Burnham, N. A.; Kulik, A.; Vogel, H.; Duschl, C. *Langmuir* **1997**, 13, 2425-8.
[6] Wong, S.-S.; Porter, M. D. *J. Electroanal. Chem.* **2000**, 485, 135-43.
[7] Chem3D, Ultra 8.0, CambridgeSoft: Cambridge MA, 2004.
[8] Widrig, C. A.; Chung, C.; Porter, M. D. *J. Electroanal. Chem.* **1991**, 310, 335-59.
[9] Jung, H. H.; Won, Y. D.; Shin, S.; Kim, K. *Langmuir* **1999**, 15, 1147-54.
[10] a) Tao, Y.-T.; Wu, C.-C.; Eu, J.-Y.; Lin, W.-L. *Langmuir* **1997**, 13, 4018-23; b) Howell, S.; Kuila, D.; Kasibhatla, B.; Kubiak, C. P.; Janes, D.; Reifenberger, R. *Langmuir* **2002**, 18, 5120-5.
[11] Zhong, C.-J.; Brush, R. C.; Anderegg, J.; Porter, M. D. *Langmuir* **1999**, 15, 518-25.
[12] Evans, S. D.; Urankar, E.; Ulman, A.; Ferris, N. *J. Am. Chem. Soc.* **1991**, 113, 4121-31.
[13] Lide, D. R., Ed. *Handbook of Chemistry and Physics*, 76 ed.; CRC Press: Boca Raton, 1995.